Journal of Applied Fluid Mechanics, Vol. 11, No. 3, pp. 695-707, 2018.
Available online at www.jafmonline.net, ISSN 1735-3572, EISSN 1735-3645.
DOI: 10.29252/jafm.11.03.27173

An Optical Flow Measurement Technique based on Continuous Wavelet Transform

A. B. Osman[1†], M. Ovinis[1†], I. Faye[2], F. M. Hashim[1] and H. Osei[1].

[1] *Mechanical Engineering Department, Universiti Teknologi PETRONAS, Seri Iskandar, 32610 Tronoh, Perak, Malaysia*
[2] *Fundamental and Applied Sciences Department, Universiti Teknologi PETRONAS, Seri Iskandar, 32610 Tronoh, Perak, Malaysia*

†*Corresponding Authors Emails: mark_ovinis@utp.edu.my*

(Received September 9, 2016; accepted December 5, 2017)

ABSTRACT

Flow measurement underwater oil leak is a challenging problem, due to the complex nature of flow dynamics. Oil jet flow associated with a multi-scale coherent structure in both space and time direction. Optical plume velocimetry (OPV) was developed by (Crone, McDuff, and Wilcock, 2008), and it was the most accurate technique that used for oil leak flow measurement. Despite its better estimation, the OPV measured the oil flow rate with high uncertainty of 21%. This is due to the multi-scale phenomena of oil flow, as well as the limited accuracy of direct cross correlation (DCC) typically used by OPV. This paper proposed a novel technique that considers the multi-scale property of turbulence in flow measurement. The proposed technique is based on continuous wavelet transform and estimates the flow using the following steps: Decomposition of turbulent flow signal by using continuous wavelet transform (CWT), correlation coefficient estimation in which Fast Fourier Transform (FFT) algorithm was used, interpolation and peak detection for the estimated correlation coefficients, and finally, the velocity field estimation. In order to validate the CWT-based technique, a turbulent buoyant jet, which has a similar flow-type of oil jet was experimentally simulated. Then, the CWT-based technique was applied to measure the jet flow, and the outcomes of the technique was compared to the experimental results. As a result, utilizing a smaller number of wavelet scales lead in better flow measurement as compared to the use of larger scales. CWT-based technique was accurately estimated the jet flow rate with standard error of 0.15 m/s, and outperformed the classical algorithms, including FFT, and DCC algorithms, which were measured with error of 3.65 m/s and 4.53 m/s respectively.

Keywords: Multi-scale; Turbulent signal decomposition; Wavelet transform; Optical technique.

NOMENCLATURE

A	nozzle cross sectional area	SE	standard erro
a, b	wavelet dilatation and shift parameters	t	time
B	bouncy flux	U	nozzle inlet velocity
d	distance	U_m	centerline velocity
F, f, g	generic functions	V	estimated nozzle velocity
l_M	morton length scale		
M	momentum flux	τ	time delay
Q	nozzle flow rate	σ	standard deviation
R	cross correlation coefficient	ρ	density

1. INTRODUCTION

Flow measurement of an oil leak is an important issue for optimal design of avoiding leak disasters and for good plan of minimizing its dangers (Marcia K McNutt *et al*., 2012). Estimation of oil leak volume is usually based on analyzing the data of remote sensing that is collected from sea surface (Brekke and Solberg, 2005; Jha, Levy, and Gao, 2008). However, estimation from sea surface has several drawbacks: first, weather conditions play an important role for the quality of the leak data, which will directly affect the accurate of oil estimation. Second, the difficulty of identifying the thickness of oil slick, which is essential factor for volume estimation (Fingas and Brown, 2014). Third, from

sea surface only the amount of oil below sea level can be quantified, while large amount of oil remains underwater. Therefore, the theory suggest that quantification of oil leak volume from underwater source has been more reliable than estimating based on the surface.

Due to the lack of flow measurement techniques for oil leak estimation several techniques (e.g. acoustic technique, and video based techniques) were used in case of Macondo well incident in 2010. These techniques were developed for flow measurement in laboratory scale, and have been applied to quantify the amount of oil spill in the Macondo well (Marcia K McNutt *et al*., 2012). Video-based techniques or "optical techniques" have a degree of advantage over acoustic technique and these include the former's low cost and easier application in both sea surface and the underwater environment over the latter. Optical techniques are based on estimating the velocity field based on video or image sequence data recorded by optical sensors. Several optical techniques have been applied for underwater oil spill flow estimation. This include manual tracking of fluid features, such as using Feature Tracking Velocimetry (FTV) and Large Eddy Velocimetry (LEV), to automatic estimation such as Particle Image Velocimetry (PIV) and Optical Plume Velocimetry (OPV) (Marcia K McNutt *et al*., 2012). FTV and LEV estimate the velocity based on manual tracking of the existing fluid feature in video data (e.g. coherent structure) (Lehr *et al*., 2010). However, these techniques poorly estimated the flow rate of the oil leak (Marcia Kemper McNutt *et al*., 2011), because of the difficulty to track the visible features of the turbulent flow from one video frame to another. Despite the acceptable accuracy of the PIV technique when used to estimate the velocity field of fluid from experimental (Adrian, 2005), the use of PIV for underwater spill estimation resulted in underestimation by a factor two (Lehr *et al*., 2010). There are two reasons for the inaccurate result of PIV when used in underwater oil spill estimation: First, an oil spill is optically too dense, rendering ineffective the cross correlation algorithm that is usually used with the PIV technique to estimate the particle displacement. Secondly, the standard interrogation windows of PIV are limited, resulting in the inability of the technique to capture large motion between image frames.

The most accurate technique found for oil volume estimation is OPV (Crone et al., 2008). The technique was developed to estimate the flow rate of underwater hydrothermal vent. The reason behind the better accuracy of OPV over other optical techniques is that OPV is based on temporal averaging in which the temporal variation of the fluid turbulent flow is considered, while PIV, FTV, and LEV are based on spatial correlation using two consecutive images only for velocity estimation. While both OPV and PIV use a standard cross correlation algorithm for image velocity estimation, PIV fails to estimate the oil flow rate accurately (Marcia K McNutt *et al*., 2012). This is because PIV implements the cross correlation algorithm spatially between two consecutive images and has been used for real turbulent flow estimation of hydrothermal vent while OPV considers the time variation (i.e. temporal averaging) of fluid flow and implements the cross correlation algorithm temporally (Crone, Wilcock, and McDuff, 2010).

Moreover, the use of temporal averaging has many advantages over spatial averaging or spatial-temporal based methods. It is less time consuming, has no loss of spatial information and is able to estimate velocity in all turbulent flow space. Staack *et al*.(Staack, Wereley, Garbe, and Willert, 2012) compared seven algorithms which included the most available ones at that time, temporal correlation, spatial correlation and optical flow algorithms. In their work, temporal cross correlation outperformed the other algorithms when used for estimating the velocity field of turbulent buoyant jet flow simulated experimentally, and with actual data of an underwater oil spill. Likewise, the temporal averaging has been applied in velocity estimation of turbulent flow for several flow measurement techniques, such as Hot Wire Anemometry (HWA) (Bruun, 1996; Comte-Bellot, 1976), and Laser Doppler Velocimetry (LDV) (Meier and Roesgen, 2012).

In fact, the turbulent flow has multi-scaling properties in both space and time, and its motion occurs in a wide range of length scales, and a wide range of time scales (Taylor, 1935).The scaling properties of a turbulent jet over its three regions is not similar. For example, the fully developed region includes a large range of turbulent length scales (i.e. bigger sizes of vortices), while in the pure jet region, the flow is almost translating without rotation in the flow direction, and the transitional region is a mixed region between the higher range of scales of fully developed region and the very small scales in pure jet of turbulent jet. This could be the reason for the inaccurate results of the OPV technique in the pure and transitional regions. The behavior of turbulent flow over time can be described as a non-stationary signal in which its statistical properties (i.e. mean, standard deviation) are not constant over time. This signal includes lower and higher peaks of variable amplitudes, and the density of the peaks vary from time to time, with short-time and long-time fluctuations. A method that considers the scale and time information of turbulent flow is therefore required when estimating its velocity field.

In this respect, wavelet transforms would be a powerful tool for analyzing the multi-scale phenomena of turbulent flow. It has previously been used by (Farge, 1992) for analyzing the non-stationary behavior of turbulent signals. The continuous wavelet transform has the ability to decompose a signal into many scales, with maintaining its time information as well. Extensive works have been conducted on using wavelet transforms to study turbulent flow starting with the work of (Farge, 1992), who reviewed the wavelet transforms used in turbulence applications, and a more recent work on analyzing turbulent flow using wavelet transform (Debnath and Shah, 2015). Fu *et*

al. (Fu, Agarwal, Cavalieri, and Jordan, 2016; Kanani and da Silva, 2015; Li, 1998) studied the coherent structure of a turbulent flow, and Xu *et al*. (Xu, Wan, and Zhang, 2006) applied wavelet transform to investigate the self-similarity and intermittency property of plasma phenomena of turbulent flow. To the best knowledge of authors, the use of wavelet transforms in the fluid dynamic field is used in analyzing turbulent flow where the velocity field is known(Buresti, Lombardi, and Bellazzini, 2004). Dérian *et al*. (Dérian, 2012; Dérian, Héas, Herzet, and Mémin, 2013; Dérian, Héas, Herzet, and Mémin, 2011) applied a 2D discrete wavelet transform by combing the classical optical flow algorithm for fluid flow estimation from image sequences. They found that the use of wavelets resulted in a better flow estimation.

In this paper, a novel technique is proposed for estimating the velocity field and the flow rate of a simulated underwater oil spill flow. The proposed technique is based on the scaling properties of the turbulent signal, by decomposing the signal into multiple scales using the CWT. The rest of the paper is organized as follows: Section 1 briefly describes the fundamental of turbulent buoyant jet flow; Section 2, the basics of wavelet transform followed by the overall description of the proposed method; Section 3 gives the details of the experimental work and Section 4presents the results and discussion followed by the conclusion.

2. METHOD

The following section outlines the general methodology for this paper, includes a theoretical background about the turbulent jet flow and the fundamental of wavelet transform. Followed by a description for the proposed wavelet technique as well as the procedures for experimental work.

2.1 Theory of Turbulent Buoyant Jet

Underwater oil leak has the characteristic of a turbulent buoyant jet, in which two fluids with different densities mix together, with the jet having an initial moment and buoyancy energy. The jet flow dynamics is usually affected by the initial conditions at the jet nozzle (e.g. flow rate at the nozzle, nozzle size, and nozzle shape) (Lipari and Stansby, 2011). This jet flow has three regimes in the flow direction, namely pure jet, transitional and fully developed region. For each regime, the velocity profile has a certain trend. In the pure jet region, the momentum flux, M can be calculated using the following equation (Mcduff, 1995):

$$M = QU = AU^2 \tag{1}$$

where Q is the flow rate of the nozzle, A is its cross sectional area, and U is the nozzle velocity. And the mean centerline velocity, Um in the stream-wise direction is given by (Turner, 1986):

$$U_m = kM^{1/2}x^{-1} \tag{2}$$

Where k is a constant equal to 7, x is the distance in stream-wise direction from the virtual origin of the jet. Therefore, the mean velocity in radial direction, v of the jet in any distance x from the nozzle is given by (Turner, 1986):

$$v = U_m \exp\left[-\left(\frac{r}{b}\right)^2\right] \tag{3}$$

where b is constant and has been experimentally found to be $0.1x$, where r is the radial distance.

Far from the nozzle, the turbulent buoyant jet acts as a pure plume in which the buoyancy force is the only force controlling the jet flow based on the density difference of the two fluids. The buoyancy flux B at the nozzle is given by (Papanicolaou and List, 1988):

$$B = g\frac{\Delta\rho}{\rho}Q \tag{4}$$

where, g is the gravitational acceleration, $\Delta\rho$ the density difference between plume and ambient fluid, ρ is the ambient fluid density, and Q is the flow rate. The mean velocity in stream-wise direction of the plume (Turner, 1986) can be expressed as shown in Eq. (5):

$$U_m = c_1 B^{1/3} x^{-1/3} \tag{5}$$

Where C_1 is a constant experimentally found to be in the range of 3.4 to 3.9 (Turner, 1986). Therefore, the mean velocity in the radial direction, has a similar form in terms of equation as the pure jet case, as described by Papanicolaou (Papanicolaou and List, 1988).

Between the pure jet and pure plume regions in turbulent buoyant jets, there is a transition region. A dimensionless distance, x/l_M is usually used for identifying this region, where l_M is the Morton scale and is given by Eq. (6) (Turner, 1986):

$$l_M = \frac{M^{3/4}}{B^{1/2}} \tag{6}$$

In the case where $x/l_M < 1$, it is pure jet region; where $x/l_M > 5$, it is pure plume and in between these two ranges, it is transition region (Papanicolaou and List, 1988).

2.2 Fundamental of Wavelet Transform

Wavelet transforms are powerful tools for analyzing non-stationary signals such as turbulent signal, and have the ability to represent the signal time variation as well as its frequency content. Figure 1 shows a comparison of the common domains for representing any signal. In the time domain, only the signal amplitude is available without frequency content (represented by vertical lines), and vice versa in the frequency domain, in which only the frequency content of the signal is known, while the signal amplitude is lost (represented by horizontal lines). The Short Time Fourier Transform (STFT), also known as the Gabor transform, is an option for representing the signal in both time and frequency domain using the window function and time translation. The length of the window function

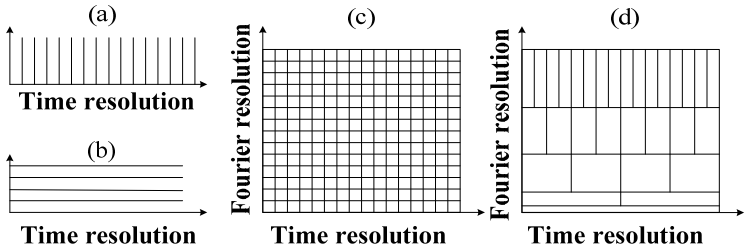

Fig. 1. Comparison between signals representation methods (a) time domain (b) frequency domain (c) and (d) wavelet domain.

decreases as the time resolution increases. However the frequency resolution reduces, or vice versa. This means that the time resolution and the frequency resolution for all frequency and time instant become fixed for fixed window. STFT exhibits equal resolution of time and frequency (see Fig. 1-b).The disadvantage of STFT is the use of constant time and frequency resolutions which are independent of each other. Wavelet transform on the other hand, is a multi-resolution technique which presents the signal in several scales by using a windowing scheme that adapts to the time frequency. As such wavelet transform is ideal for representing the turbulent signals since these signals exhibits transient and random variations in frequency content.

2.3 Image Velocity Field Estimation

The proposed technique in this work estimates the image velocity field from a sequence of images by cross correlating two points with a known distance in turbulent space. By estimating the time delay between the signals of the two points, the velocity can be estimated (by dividing the distance over time). By repeating the same steps for other points in turbulent flow space, the overall velocity field of the turbulent jet can be estimated. As shown in Fig. 2, the first step for velocity field estimation is for selecting two points which are separated by a known distance *d* in the turbulent jet space. The intensity value of those two points is a signal which has a length equal to the number of images used. By knowing the distance *d* between two points in the turbulent jet space, as well as the time delay *t* estimated using the methods described in the previous sections, the velocity *V* can be estimated from the following equation:

$$V = \frac{d}{t} \tag{7}$$

where *V* is the velocity (m/sec), *d* is the selected correlation distance, and *t* is the time delay.

The accuracy of velocity estimation is based on both proper selection of the correlation distance *d*, and the accuracy of the method used for time delay estimation. Figure 2 shows the overall steps for velocity estimation. Firstly, a distance of 5 pixels is fixed for all cases of flow rates. Secondly, time *t* will be estimated in wavelet domain and requires several steps – transforming the turbulent signals in the wavelet domain using CWT to decompose the signals into many scales, cross correlation of the CWT coefficients of each scale using FFT algorithm, interpolation of the resultant correlation coefficient, and the required time obtained by detecting the peak of the interpolated coefficients. This will result in a set of time delay whose number is equal to the number of CWT scales that was used to decompose the signals, and the final time delay is estimated by averaging of these delays. The next subsections describes the steps for estimating time delay, velocity field, and flow rate of a turbulent buoyant jet from image sequences.

2.3.1 Continuous Wavelet Transform

Continuous wavelet transforms (CWT) is a powerful time-scale technique used to decompose a signal into multi-scale. CWT was applied to decompose turbulent signals extracted from image sequences into several scales. As shown in Figure 2, the CWT matrix presented time-domain signal into multi-scale with providing the local time information of the signal. In the time domain, the frequency cannot be provided, because only the signal amplitude could be observed. While in frequency domain (such as using the Fourier transform) only frequency information has existed while the FT has a problem of time resolution. To use of CWT, both time-domain and frequency-domain information about the signal can be provided. CWT matrix for any turbulent signal was obtained by cross correlation between the signals with a defined mother wavelet function producing a CWT coefficient.

This is lead to sample the turbulent signal at each scale wavelet, in which lower scales have higher sampling frequency, while the higher scales associated with lower sampling. The scaling and sampling properties are an important factor for signal correlation. Then, by estimating a time delay between each wavelet scale, the final velocity field can be estimated The CWT of a time domain signal, *f(t)* is given by Eq. (8):

$$W_g(b,a) = \frac{1}{\sqrt{a}} \int_{-\infty}^{\infty} f(t) g^* \left(\frac{t-b}{a} \right) dt \tag{8}$$

where *a, b* are the dilatation and shift parameter respectively, * denotes complex conjugate and *g(x)* is the mother wavelet function.

For wavelet function, four commonly used functions were selected for comparison purpose, including Morlet, Gaussian, Symlet, and Mexican-hat.. The selection of these wavelets is based on the

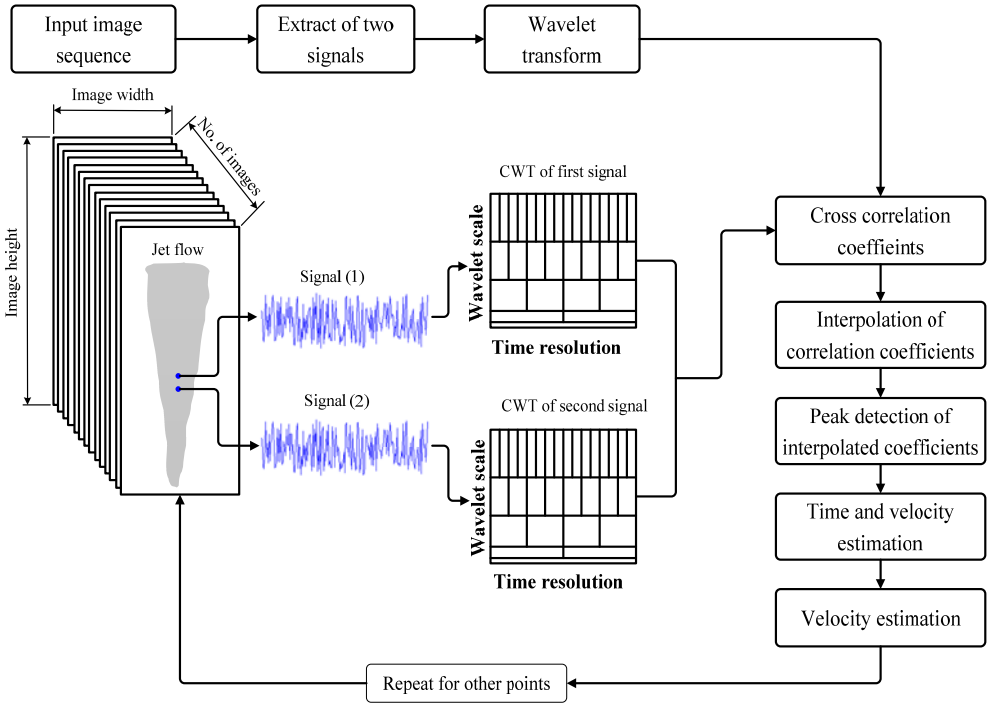

Fig. 2. Continuous wavelet based algorithm used for image velocity field estimation.

work of (Farge, 1992), and for their advantages in providing local information of input signals. This may lead to improve the accuracy of image velocity field estimation. . Morlet is a good function which provides local periodicity of signal, Mexican-hat is a good for local structure, while Gaussian wavelet is used for identifying local gradients of signals (Gordeyev, 2000).

The Morlet wavelet function is defined by:

$$g(x) = \exp(ibx)\exp(-x^2/2), b \geq 5 \tag{9}$$

The Mexican-hat wavelet is given by:

$$g(x) = \frac{d^2}{dx^2}\exp(-x^2/2) \tag{10}$$

and the Gaussian wavelet in the first derivative form is defined by:

$$g(x) = \frac{d}{dx}\exp(-x^2/2) \tag{11}$$

2.3.2 FFT Cross Correlation

One of the important steps for velocity estimation is time delay estimation, which requires estimation of the correlation coefficients between the selected CWT scales of the signals collected from two points in turbulent flow space (see Fig. 2). FFT-cross correlation algorithm is used for correlation coefficient estimation between each CWT scale individually. The FFT-cross correlation is a classical algorithm for similarity measure between two signals/images and is used in many applications such as time delay estimation(Gilbert and Johnson, 2003) and PIV (Pust, 2000). Figure 3 shows the block diagram of a FFT cross correlation. The correlation estimation between any two signals x_1 and x_2 sing a FFT cross correlation algorithm requires three steps. The first involves the Fourier transform of the two signals which are multiplied, then the inverse the FFT of the multiplication results, followed by peak detection to obtain the delay, D.

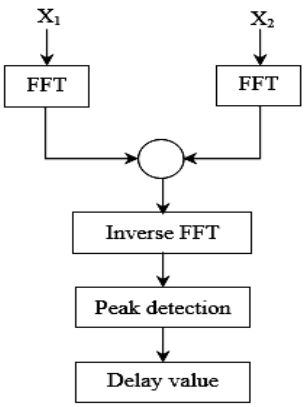

Fig. 3. Time delay estimation between two signals x_1 and x_2 using FFT cross correlation algorithm.

The FFT - cross correlation can be written as:

$$R_{FFT}(\tau) = FFT(x_2).*(IFFT(x_1) \tag{2}$$

where τ is the time delay between the two signals, * denotes the complex conjugate. The Fast Fourier transform (FFT) of a signal with a function *f(n)* with length of *n* is given by:

$$F(x) = \sum_{n=0}^{N-1} f(n) e^{-j2\pi(\frac{n}{N}x)} \tag{13}$$

And the inverse of FFT is given by Eq. (14):

$$f(n)=\frac{1}{N}\sum_{n=0}^{N-1}F(x)e^{-j2\pi(\frac{n}{N}x)} \tag{14}$$

Where *F(x)* is represent the signal $f(n)$ in frequency domain.
The correlation coefficient also can be estimated using direct cross correlation (DCC) in time domain using the following Equation:

$$R_{DCC}=\sum_{i=1}^{N-1}s(t)s(t+\delta t) \tag{15}$$

where δt is the first signal, and $s(t+\delta t)$ is the delayed signal by amount of δt .

2.3.3 Interpolation of Correlation Coefficients

Interpolation of the obtained correlation coefficients is required for accurate detection of coefficients peaks. This will lead to improve the accuracy in time delay estimation as well as the final velocity field. In this work a parabolic interpolation (Wiens and Bradley, 2009) was applied to find the fraction of time delay. The parabola fitting has the advantage of better accuracy and can be used with less computational complexity (Jacovitti and Scarano, 1993; Wiens and Bradley, 2009). To interpolate the peak of correlation coefficients, the parabola interpolation model is given by Eq. (16):

$$\hat{t}_d=k+\frac{xc_{01}(k-1)-xc_{01}(k+1)}{2(xc_{01}(k-1)-2xc_{01}(k)+xc_{01}(k+1)} \tag{16}$$

Where $xc_{01}(k)$ is the peak of the real correlation coefficient, and $xc_{01}(k-1), xc_{01}(k-1)$ are the two neighbors of peak point of correlation coefficients.

The final step for time delay estimation is by detecting the interpolated peak of correlation coefficients. The required time delay is the delay that corresponds to this peak, as expressed by the following equation:

$$D_{FFT}=\arg_t\max|R(\tau)| \tag{17}$$

The delay estimation from CWT scales will result in a number of delays that is equal to the number of selected scales. Then, an averaging of these delays is required to find the final time delay to use for velocity estimation. However, the estimated delays gave small and large values when compared to the rest of the delays and they can be treated as outliers. The direct averaging of the estimated delays is susceptible to the influence of outliers. Several approaches had been used for removing data outliers which were reviewed by Walfish *et al.* (Walfish, 2006). However in this work, statistical based approach was used to remove the outliers of estimated time delays. The approach removed the data outliers by defining the upper and lower limits of the useful data by subtracting and adding three times of its standard deviation from the mean delay using Eq. (18).

$$D=\overline{D}\pm 3\sigma \tag{18}$$

where $\overline{D}$ is the mean delay, and σ is the standard deviation.

So, the final time delay estimation is the average delay of all time delays estimated between the CWT scales using an equation after removing the outliers of delays. Figure 4 shows the idea for removing the outliers of estimated time delays.

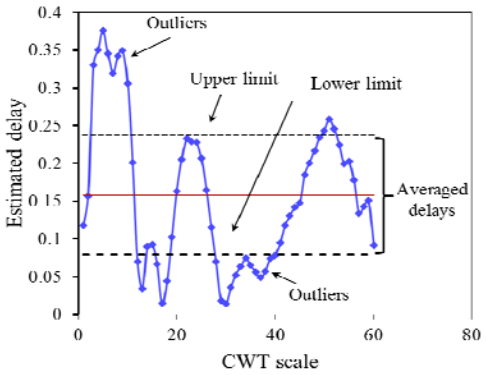

Fig. 4. Time delay outliers removing and averaging process.

First the average of estimated delays from each CWT scales was calculated (red line), then the lower and upper limits of the acceptable delays were calculated (black dash lines). Finally, the required time was calculated as the average of delays in the range between lower and upper limits.

2.4 Flow Rate Estimation

The nozzle flow rate was estimated by multiplying the cross sectional area of the nozzle by the nozzle velocity, where the nozzle velocity obtained from the image velocity field. The nozzle flow rate can be expressed by the following equation:

$$Q=AV \tag{19}$$

where Q is the nozzle flow rate, A is the cross-sectional area of the jet, and V is the nozzle velocity.

The estimated velocity field is a two-dimensional matrix, which requires to be averaged and converted from pixel unit to metric scale. Several averaging approaches can be proposed to get the final value of V in meter per second. Averaging of all image velocity vectors, averaging the velocities in a certain region of velocity field space, by threshold the image velocity and reject the velocity vectors outliers and apply averaging to the remaining vectors. Based on the theory of turbulent buoyant jet discussed in Section 2.1, the velocity field in the near nozzle region are closer to the value of actual nozzle velocity. Then the nozzle flow rate can be accurately estimated. Therefore, the estimation of the nozzle flow rate by averaging of the velocity vectors of the near nozzle region might results in accurate estimation with closer

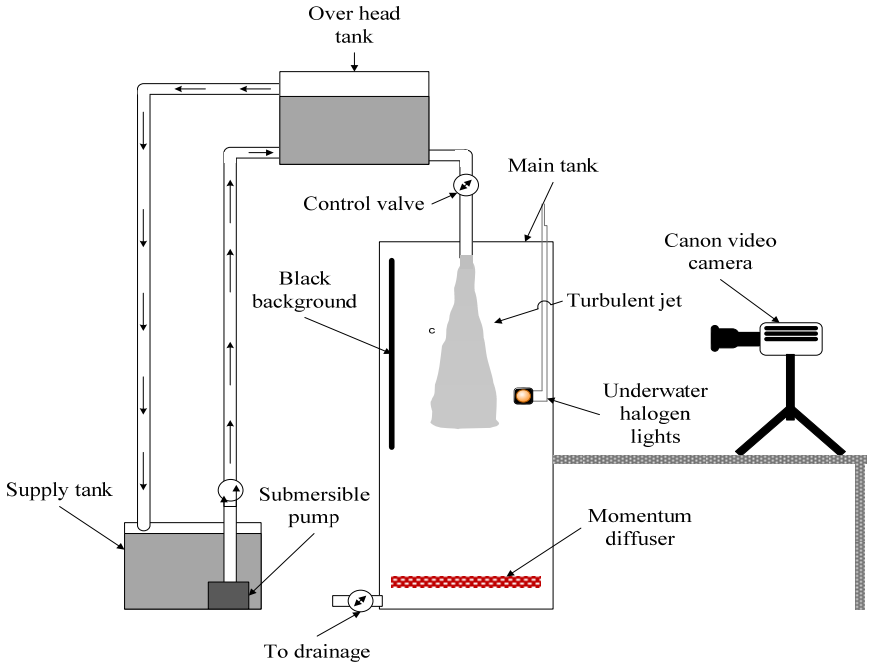

Fig. 5. Experimental rig set-up used for turbulent buoyant jet simulation.

value to the measured experimental value. In this work, and based on our investigation better estimation of nozzle velocity can be done by averaging of velocity vectors by taking a rectangular region in the near nozzle region of turbulent jet flow with a size of horizontal distance equal to nozzle diameter (d) and vertical distance equal to twice of the nozzle diameter (2d).

The standard error *(SE)* between experimental nozzle flow rate and the estimated flow rate is defined as:

$$SE = \frac{\sigma_{N-1}}{\sqrt{N}} \tag{20}$$

In which the standard deviation σ_{N-1} is given by:

$$\sigma_{N-1} = \sqrt{\frac{1}{N-1}\sum (V - \overline{V})^2} \tag{21}$$

Where $\overline{V}$ the average velocity, and N is the number of measurement.

2.5 Laboratory Work

To develop the optical flow measurement technique, an experimental work was conducted. A turbulent buoyant jet was experimentally simulated with three different ranges of nozzle flow rates. Then, a video camera was used to capture the jet flow Therefore, the main goal is to estimate the image velocity as well as the nozzle flow rate from the collected video using the developed algorithm and compare with the experimental values.

Figure 5 illustrates the experimental rig set-up that used for turbulent buoyant jet simulation. This set-up is almost similar to the set-up of Crone *et al.* (Crone *et al.*, 2008) who developed OPV. The set-up consists of three tanks, supply tank, overhead tank and the main tank. The main tank made of transparent acrylic and had dimensions of 900x900x2000 mm. The large size of the main tank to avoid the flow touching the walls. The overhead tank is used to provide a constant flow rate when the control valve was opened by maintaining a constant water level. To conduct experimental run, first, the supply tank was filled with a mixture of tap water, colloidal graphite for better visualization of the flow as well as salt with 5 % weight in order to provide the buoyancy effect to the simulated turbulent buoyant jet flow.

For each experimental run, the flow control valve was used to control the nozzle flow rate. A submersible pump was placed into the supply tank in order to supply the mixed fluid and deliver to the overhead tank. By controlling the flow control valve, the mixed fluid flows from overhead tank through a nozzle had a diameter of 8-mm to the main tank leading to a turbulent buoyant jet simulation. A momentum diffuser was fixed at the bottom of the main tank in order to keep the mixed fluid to be at the bottom of the tank. The selection of lights with an appropriate wavelength is an important factor for flow visualization. Two underwater halogen lights with a wavelength of 450 – 500 nm were used. For a better visibility of the turbulent jet flow, a black background was used. Finally, in order to convert the pixel into metric unit, a check-board had a size of10x10mm used.

Three experimental runs were conducted with six cases of jet nozzle flow rates and video of the turbulent jet flow was recorded. Two types of video cameras were used, a Phantom 9.1 high speed camera, and a Canon EOS-550 video camera. However, only three flow rate cases from the Canon camera data were analyzed in this work, in order to

evaluate the accuracy of the proposed technique. By adjusting the distance of the camera from nozzle, the focal length, and the focusing level, the camera field of view was adjusted to include all flow regimes of the turbulent jet (i.e. pure jet, transitional, and fully developed regime). The Canon video camera was used to record a 20 sec video for each experimental run, using a frame rate of 50 fps with a resolution of 1280×720 pixels and a standard focal length of 50 mm. The total useful number of frames recorded for each run was between 4000 - 6000 frames.

Figure 6 shows a typical sample image from a higher flow rate video, the average of 1000 image sequence. To estimate the velocity in the flow area, the jet boundary was segmented using Otsu's thresholding method (Otsu, 1975) from the average of the image sequence. Table 1 summarizes the three cases of flow rates considered in this work. For each flow rate, the control valve was calibrated and the time for one liter of the mixed fluid to flow was measured using a stop-watch, and the flow rate Q_i was calculated. The average flow rate Q_m with its standard deviation σ and standard error (*SE*) were calculated.

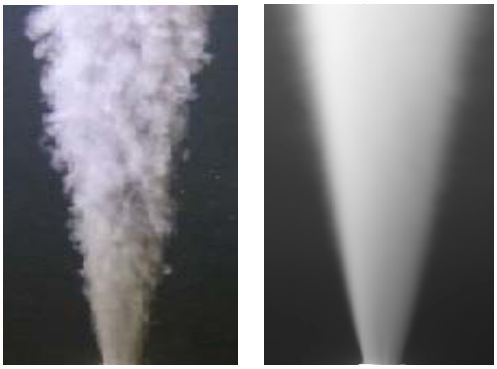

Fig. 6. (a) Sample of original image (b) average of 1000 image sequences.

Table 1 Summary of flow rate measurements for experimental works

No.	t	Q_i (l/s)	Q_i (m^3/s) x 10^{-3}	Q_m (m^3/s) x 10^{-3}	σ	SE
1	39	0.026	0.026	0.027	1.58	0.71
	38	0.026	0.026			
	35	0.029	0.029			
	36	0.028	0.028			
	37	0.027	0.027			
2	19	0.053	0.053	0.054	0.96	0.48
	20	0.05	0.05			
	18	0.056	0.056			
	18	0.056	0.056			
3	10	0.10	0.10	0.091	0.82	0.41
	11	0.091	0.091			
	12	0.083	0.083			
	11	0.091	0.091			

Table 2 shows the velocity estimated by dividing the average flow rate Q_m over the cross section of the nozzle in m/sec and pixel/frame as well as the range of Reynold number. The velocity in frame/pixel was estimated using a scale of 4 pixels per every one millimeter obtained from check-board used for camera calibration before running the experiments.

Table 2 Estimated nozzle velocity for different Reynold number (Re) cases

Exp. Run	Velocity (m/sec)	Velocity (pixel/frame)	Re
1	0.35	27.72	3465
2	0.68	54.78	6847
3	1.16	93.00	11624

3. RESULTS AND DISCUSSION

3.1 Statistical Analysis of the Collected Data

To improve the quality of video data, a lot of efforts were done by adjusting the lights, the camera position, and the focus. One of the important factors for accuracy and performance of the proposed technique is the proper selection of the number of images used for velocity estimation. More image sequence leads to reduce the statistical error at the expensive of computational time.

Figure 7 shows the relation standard errors estimated at two points in the jet flow space against using various number of images. Increasing the number of images leads to reduction in error. The statistical error is mainly based on the number of images (i.e. sampling). However, the increasing number of images used in the velocity estimation increased the time for uploading these images into the 3D matrix and needed more capacity of ram. The error was almost constant after 1000 images, therefore, 1000 images was used in this study.

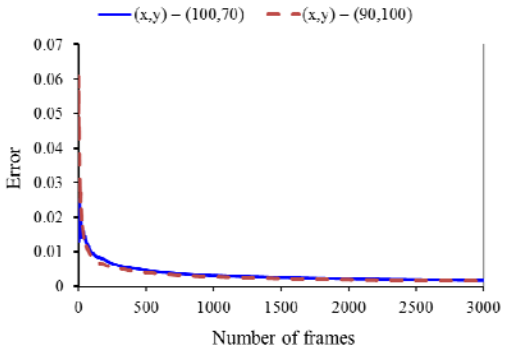

Fig. 7. Standard errors VS number of images.

3.2 Evaluation of Optical Technique

Several factors affected the accuracy of developed technique, such as the number of CWT scales used for decomposing the signals, and the mother wavelet function used for scaling the signal. Different number of scales and different mother wavelet functions were used. In this section, the effect of these factors on the accuracy of the technique for estimating the velocity field of turbulent jet is presented and

discussed, as well as a comparison of the final velocity field and flow rates estimated using the wavelet based technique compared with the results based on FFT and DCC algorithms without wavelet decomposition as well as the theoretical velocity field of turbulent jet.

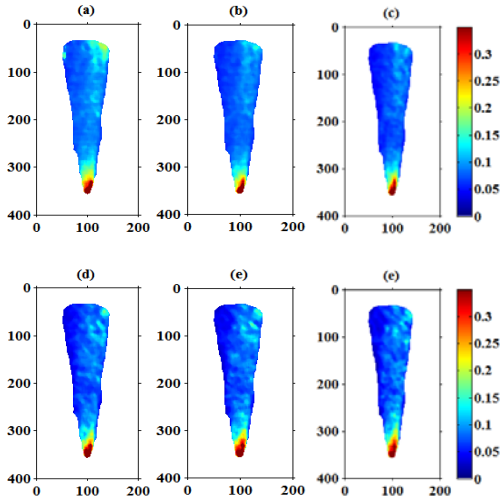

Fig. 8. Estimated image velocity field using various wavelet scales (a) 5 scales, (b) 10 scales, (c) 20 scales, (d) 40 scales, (c) 60 scales and (e) 80 scales for flow rate case of Q_1.

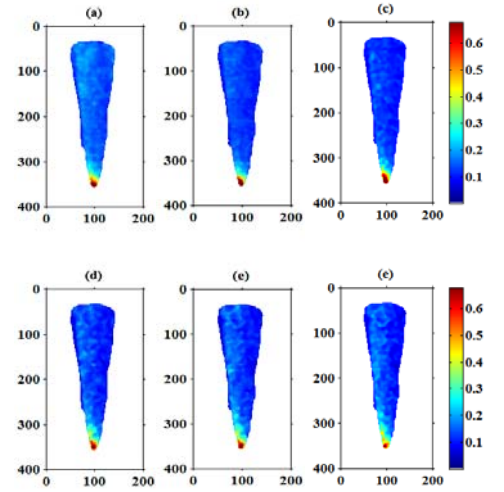

Fig. 9. Estimated image velocity field using various wavelet scales (a) 5 scales, (b) 10 scales, (c) 20 scales, (d) 40 scales, (c) 60 scales and (e) 80 scales for flow rate case of Q_2.

3.2.2 Effect of Number of Wavelet Scales

One of the important factors that may affect the accuracy of the proposed technique is the number of CWT scales used for decomposing the turbulent signals. By using the Morlet wavelet function, the velocity field of turbulent jet was estimated for different number of CWT scales ranging from 5, 10, 20, 40, 60, and 80 scales. Figure 9 shows the estimated velocity field for each case. Generally, the use of lower number of scales (e.g. a = 5) resulted in noisy velocity field. However, similar velocity fields were observed in cases of using middle scales when compared to other values. By increasing the number of scales, the velocity magnitude in the far jet region increases slightly, and lack of symmetry for the velocity distribution increases. This observation for cases of flow rates are as shown in Figs. 8, 9, and 10.

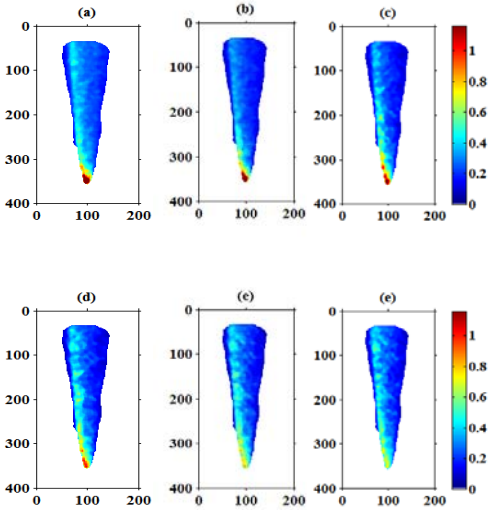

Fig. 10. Estimated image velocity field using various wavelet scales (a) 5 scales, (b) 10 scales, (c) 20 scales, (d) 40 scales, (c) 60 scales and (e) 80 scales for flow rate case of Q_3.

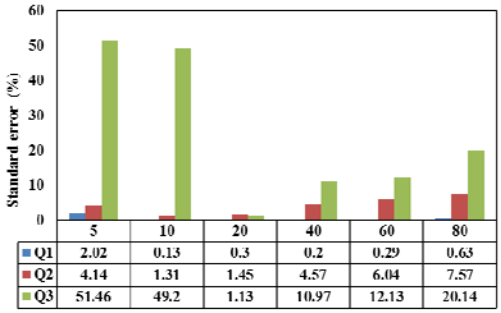

	5	10	20	40	60	80
Q1	2.02	0.13	0.3	0.2	0.29	0.63
Q2	4.14	1.31	1.45	4.57	6.04	7.57
Q3	51.46	49.2	1.13	10.97	12.13	20.14

Fig. 11. Relative errors in the estimated flow rate for various wavelet scales.

Figure 11 shows the estimated errors in flow rate estimation using the wavelet based technique by using different number of CWT scales. Generally the use of small or large number of CWT scales resulted in a large errors, and the higher flow rate value led to decreasing accuracy of the technique. For an example, for Q_1, an error of 1.13% resulted by using 20 scales as compared to an error of 51.5% where the scales were 5, and an error of 20.14% when there were 80 scales. The small number of scales means small range of sampling frequency for CWT scales and the existence of noise with most of these scales. The large number of scales means large range of sampling frequency which leads to wrong correlation between CWT scales in the higher level (Mallat, 1999). These two reasons leads to wrong time delay estimation between each CWT scale of the two signals, affecting the accuracy of

the flow rate estimation.

3.2.2 Effect of Mother Wavelets

The selection of mother wavelet or scaling function is an important factor for scaling any signal, and for correlation coefficient estimation between each scale for the two CWT matrices. Four mother wavelet functions (Symlet, Morlet, Gaussian, and Mexican-hat) were selected for velocity estimation and for the purpose of comparison of their final flow rate values. Figure 12, shows the velocity distribution of a turbulent jet estimated using different wavelet functions.

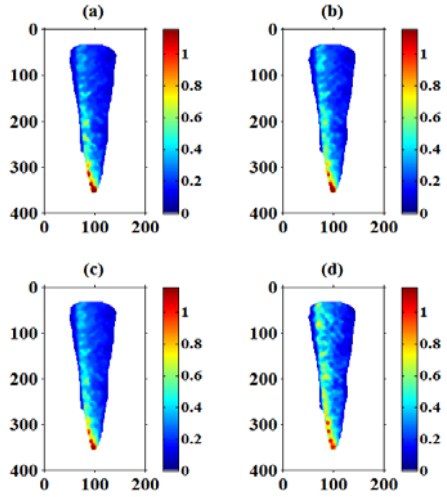

Fig. 12. Estimated image velocity field using different mother wavelets (a) Symlet wavelet, (b) Gaussian wavelet, (c) Mexican-hat wavelet, and (d) Morlet wavelet.

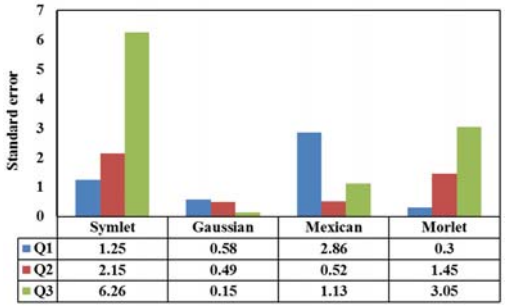

	Symlet	Gaussian	Mexican	Morlet
Q1	1.25	0.58	2.86	0.3
Q2	2.15	0.49	0.52	1.45
Q3	6.26	0.15	1.13	3.05

Fig. 13. Relative error of estimated flow rates for different mother wavelets and flow rates.

Gaussian and Morlet wavelet functions (Figs. 13 (b), (d)) resulted in almost similar velocity distribution as expected from theoretical point of view of turbulent jet flow distribution. While, un-similar velocity distribution resulted using Symlet, and Mexican-hat wavelets (Figs. 12 (a), (c)). This result confirmed the importance of proper selection of wavelet function for turbulent velocity estimation. The turbulent signals behavior was more correlated with the Gaussian and Morlet wavelets than other wavelets.

Figure 13 shows a comparison of errors in flow rate estimation as compared to the measured experimental flow rates.

The maximum standard error was 6.25 m/s when Symlet mother wavelet was used, while the other wavelet functions produced minimum errors. The most accurate result was obtained using the Gaussian wavelet function, 0.16, 0.58, and 0.58 for the case of flow rate of Q_1, Q_2, and Q_3 respectively. By increasing the flow rate of the turbulent jet, less error was obtained using the Gaussian wavelet function while, the Symlet, Morlet and Mexican function results showed high and unstable errors. The variation of errors is a result of a discrepancy in the properties of selected mother wavelets, such as center frequency which controls the sampling of wavelet coefficients in each scale of the CWT matrix, as well as the wavelet structure (Eqs. (2), (3), and (4)).

3.3 Comparison to Other Techniques

The most accurate result was obtained by using a Gaussian wavelet with 20 scales of CWT. To test the robustness of the technique, two methods were selected for the purpose of comparison, the Direct cross correlation (DCC) and the Fast Fourier Transform (FFT) cross correlation methods. Both methods estimate velocity field based on temporal cross correlation of two points in the turbulent space. However, DCC (Equation 8) relies on cross correlation in the time domain, while the FFT (Eq. (5)) is based on cross correlation in the frequency domain.

For easy comparison of the velocity fields of the wavelet based technique with the results obtained using the DCC and FFT methods, the resulting velocity matrices were normalized to the maximum velocity value obtained by each method. The three methods were compared with the predicted jet velocity distribution.

As shown in Fig. 14, the wavelet based technique results are more acceptable in which the maximum velocity is obtained in the pure jet region with the velocity gradually decaying away from the nozzle as predicted by the theory of turbulent jet velocity distribution (see Fig. 14 (d)). However, noisy velocity vectors (i.e. white color in Fig. 14 (b)) were obtained by the FFT method in the pure jet region. This noise level was reduced with the reduction of flow rate from Q_1 to Q_3. Therefore, the FFT method is more appropriate for estimation of the velocity field in case of a lower flow rate better than developed technique. The velocity distribution of the jet flow obtained by DCC method did not match with the theoretical velocity distribution of jet flow, in which most of the velocity vectors far from nozzle have similar values. Therefore, DCC could be appropriate for velocity field estimation in the pure jet region, in which higher velocity vectors were observed. This was concluded by (Crone *et al*., 2008) as well. The results of the wavelet based technique proved the ability of the technique to clearly differentiate between higher flow rate and lower flow rate (Fig. 14 (c)).

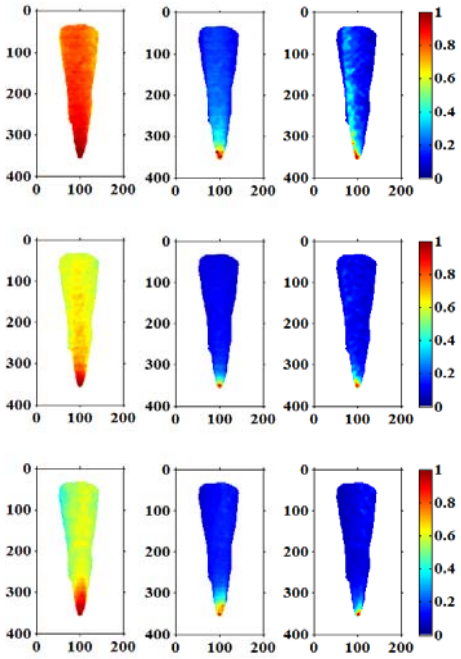

Fig. 14. Estimated image velocity field using (a) DCC method, (b) FFT method, and (c) wavelet-based technique.

Table 3 shows a comparison of the standard errors in the flow rate estimation obtained using the wavelet-based technique and other two techniques, DCC and FFT. The wavelet-based technique estimated the flow rate accurately with minimum errors by 0.15, 0.49 and 0.60 for the three cases of flow rates Q_1, Q_2, and Q_3 respectively. While higher errors obtained by both DCC and FFT methods. The wavelet based technique outperformed both the DCC and the FFT in velocity field estimation because of its ability of decomposing the turbulent signals using different sampling rates, and this helped in selecting the more reliable CWT scales for accurate time delay and velocity estimation.

Moreover, the standard deviation of the averaged velocity fields that were used for flow rate estimation was too small for wavelet based technique compared to the other two techniques. This means that most of velocities estimated using the proposed technique were close to the correct value. Larger variations of velocities around the correct value on the other hand were obtained by DCC and FFT algorithms.

Table 3 Comparison of wavelet-based technique accuracy with other techniques.

Algorithm	Q1		Q2		Q3	
	σ	SE	σ	SE	σ	SE
Wavelet	0.21	0.15	0.70	0.49	0.85	0.60
FFT	51.6	3.65	13.2	9.40	15.7	10.2
DCC	63.9	4.53	32.5	2.31	15.1	10.7

4. CONCLUDING REMARKS

An optical flow measurement technique based on continuous wavelet transform was developed. This work was motivated by the lack of dedicated technique for estimating underwater oil leak. The developed technique combined the CWT coefficients and FFT cross correlation algorithm for estimating image velocity field. To evaluate the accuracy of the technique, a turbulent buoyant jet was experimentally simulated. The jet flow was simulated with different Reynolds numbers at exist of the jet includes 11624, 6847, and 3464. Two factors affected the accuracy of the developed technique, includes the number of CWT scales that were used for scaling the two signals and the mother wavelet function used. The wavelet technique accuracy was tested with different number of CWT scales range and different wavelet functions. It was observed that, the use of 20 scales was more accurate than the others, while the use of small or large number of scales led to inaccurate results. The wavelet based method accurately estimated the flow rate with standard error ranged from 0.15 m/s to 0.6 m/s, and outperformed the two common techniques, namely DCC and FFT, which resulted in errors of 10.7 m/s and 10.2 m/s respectively for the same flow rate. However, the optical technique consumed more time (~ 2000 Sec) than the DCC and the FFT (~30 Sec).

More investigation should be made on other factors that affect the accuracy of the continuous wavelet based algorithm such as the wavelet vanishing moment, separation distance, etc. The developed technique will be evaluated using different range of nozzle flow rates. Moreover, a prediction model will be developed for the optimization of the optical technique in term of accuracy and performance.

ACKNOWLEDGEMENTS

The authors would like to express their appreciation to Universiti Teknologi PETRONAS for supporting this work under I-Gen 0153AA B30.

REFERENCES

Adrian, R. J. (2005). Twenty years of particle image velocimetry. *Experiments in Fluids 39*(2), 159-169.

Brekke, C., A. H. and Solberg (2005). Oil spill detection by satellite remote sensing. *Remote sensing of environment, 95*(1), 1-13.

Bruun, H. H. (1996). Hot-wire anemometry: principles and signal analysis: IOP Publishing.

Buresti, G., G. Lombardi and J. Bellazzini (2004). On the analysis of fluctuating velocity signals through methods based on the wavelet and Hilbert transforms. *Chaos, Solitons and Fractals 20*(1), 149-158.

Comte-Bellot, G. (1976). Hot-wire anemometry. *Annual review of fluid mechanics 8*(1), 209-231.

Crone, T. J., R. E. McDuff and W. S. Wilcock (2008). Optical plume velocimetry: A new flow measurement technique for use in

seafloor hydrothermal systems. *Experiments in fluids 45*(5), 899-915.

Crone, T. J., W. S. Wilcock and R. E. McDuff (2010). Flow rate perturbations in a black smoker hydrothermal vent in response to a mid-ocean ridge earthquake swarm. *Geochemistry, Geophysics, Geosystems 11*(3).

Debnath, L. and F. A. Shah (2015). Wavelet Transform Analysis of Turbulence *Wavelet Transforms and Their Applications* 489-516.

Dérian, P. (2012). *Wavelets and fluid motion estimation.* Université Rennes 1.

Dérian, P., P. Héas, C. Herzet and É. Mémin (2011). Wavelet-based fluid motion estimation *Scale Space and Variational Methods in Computer Vision* 737-748.

Dérian, P., P. Héas, C. Herzet and E. Mémin (2013). Wavelets and optical flow motion estimation. *Numerical Mathematics: Theory, Methods and Applications 6*, 116-137.

Farge, M. (1992). Wavelet transforms and their applications to turbulence. *Annual review of fluid mechanics 24*(1), 395-458.

Fingas, M. and C. Brown (2014). Review of oil spill remote sensing. *Marine pollution bulletin 83*(1), 9-23.

Fu, Z., Agarwal, A., A. Cavalieri and P. Jordan (2016). Extracting Coherent Structures to Explore the Minimum Jet Noise *Advances in Computation, Modeling and Control of Transitional and Turbulent Flows* 358-366 World Scientific.

Gilbert, R. and D. Johnson (2003). Evaluation of FFT-based cross-correlation algorithms for PIV in a periodic grooved channel. *Experiments in fluids 34*(4), 473-483.

Gordeyev, S. (2000). Pod, lse and wavelet decomposition: Literature review. *University of Notre Dame*.

Jacovitti, G. and G. Scarano (1993). Discrete time techniques for time delay estimation. *IEEE Transactions on signal processing 41*(2), 525-533.

Jha, M. N., J. Levy and Y. Gao (2008). Advances in remote sensing for oil spill disaster management: state-of-the-art sensors technology for oil spill surveillance. *Sensors 8*(1), 236-255.

Kanani, A. and A. M. F. Silvada (2015). Application of continuous wavelet transform to the study of large-scale coherent structures. *Environmental Fluid Mechanics 15*(6), 1293-1319.

Lehr, B., A. Aliseda, P. Bommer, P. Espina, O. Flores, J. Lasheras and O. Savas (2010). Deepwater horizon release estimate of rate by PIV. *Report to the US Dept of interior*.

Li, H. (1998). Identification of coherent structure in turbulent shear flow with wavelet correlation analysis. *Journal of fluids engineering 120*(4), 778-785.

Lipari, G. and P. K. Stansby (2011). Review of experimental data on incompressible turbulent round jets. *Flow, turbulence and combustion 87*(1), 79-114.

Mallat, S. (1999). *A wavelet tour of signal processing*: Academic press.

Mcduff, R. E. (1995). Physical dynamics of deep-sea hydrothermal plumes. *Seafloor hydrothermal systems: Physical, chemical, biological, and geological interactions* 357-368.

McNutt, M. K., R. Camilli, T. J. Crone, G. D. Guthrie, P. A. Hsieh, T. B. Ryerson and F. Shaffer (2012). Review of flow rate estimates of the Deepwater Horizon oil spill. *Proceedings of the National Academy of Sciences 109*(50), 20260-20267.

McNutt, M. K., R. Camilli, G. D. Guthrie, P. A. Hsieh, V. F. Labson, W. J. Lehr and M. K. Sogge (2011). *Assessment of flow rate estimates for the Deepwater Horizon/Macondo well oil spill*: US Department of the Interior.

Meier, A. H. and T. Roesgen (2012). Imaging laser Doppler velocimetry. *Experiments in fluids 52*(4), 1017-1026.

Otsu, N. (1975). A threshold selection method from gray-level histograms. *Automatica 11*(285-296), 23-27.

Papanicolaou, P. N. and E. J. List (1988). Investigations of round vertical turbulent buoyant jets. *Journal of Fluid Mechanics 195*, 341-391.

Pust, O. (2000). *Piv: Direct cross-correlation compared with fft-based cross-correlation.* Paper presented at the Proceedings of the 10th International Symposium on Applications of Laser Techniques to Fluid Mechanics, Lisbon, Portugal.

Staack, K., S. Wereley, C. S. Garbe and C. Willert (2012). A comparison of state-of-the-art image evaluation techniques for analysis of opaque flows.

Taylor, G. I. (1935). *Statistical theory of turbulence.* Paper presented at the Proceedings of the Royal Society of London A: Mathematical, Physical and Engineering Sciences.

Turner, J. (1986). Turbulent entrainment: the development of the entrainment assumption, and its application to geophysical flows. *Journal of Fluid Mechanics 173*, 431-471.

Walfish, S. (2006). A review of statistical outlier methods. *Pharmaceutical technology 30*(11), 82.

Wiens, T. and S. Bradley (2009). A comparison of time delay estimation methods for periodic

signals. *Digital Signal Processing, submitted September*.

Xu, G., B. Wan and W. Zhang (2006). Application of wavelet multiresolution analysis to the study of self-similarity and intermittency of plasma turbulence. *Review of scientific instruments 77*(8), 083505.